M.A. Zanchetta & R. Hillier

Blunt Cone Transition at Hypersonic Speeds: The Transition Reversal Regime

Abstract

This paper reports on an experimental investigation of transitional hypersonic boundary layers. The test geometry is a five-degree semi-angle cone. Experiments are performed in the Mach 9 Imperial College gun tunnel. Time-resolved heat-transfer rates are obtained for laminar, transitional and turbulent boundary layers, for cases in the pre-reversal and transition reversal regimes.

Introduction

Of the many problems encountered in hypersonic aerodynamics, boundary-layer transition from laminar to turbulent motion remains an elusive area, of extreme interest to the scientist and also the designer/engineer. Severe thermal loads are encountered in hypersonic flight, and vehicles often present nose blunting to attenuate the kinetic heating. The blunt-body flowfield contains sub-, tran-, super- and hypersonic regions, in which many mechanisms (Mack modes, entropy layer instabilities, nonlinear by-pass, etc.) can promote transition.

The nose-based Reynolds number Re_n is defined as the product of the unit Reynolds number $Re_\infty(\mathrm{m}^{-1})$ and the nose radius r_n. Transition studies have shown that increasing Re_n initially delays the location of transition onset and increases the length to transition, as illustrated in Fig 1. Above a certain Re_n, the transition front becomes highly three dimensional and may move upstream to the sphere-cone junction. This change in transition trend is denoted transition reversal and the range of Re_n in which it occurs is named the transition reversal regime. In this paper examples of hypersonic transition in both the pre- and reversal regime will be given.

Facility

The Imperial College number 2 gun tunnel is an intermittent facility with a 4 ms steady run window, capable of testing slender models up to 0.8 m in length. Three fully calibrated operating conditions exist, with the following nozzle exit plane conditions:

	M_∞	Re_∞ (m^{-1})	p_∞ ($\mathrm{N/m}^2$)	$T_{0,\infty}$ (K)	T_∞ (K)
low	8.89	7.51×10^6	441	1060	63.07
medium	8.93	12.62×10^6	760	1090	64.31
high	9.01	47.35×10^6	2815	1105	64.11

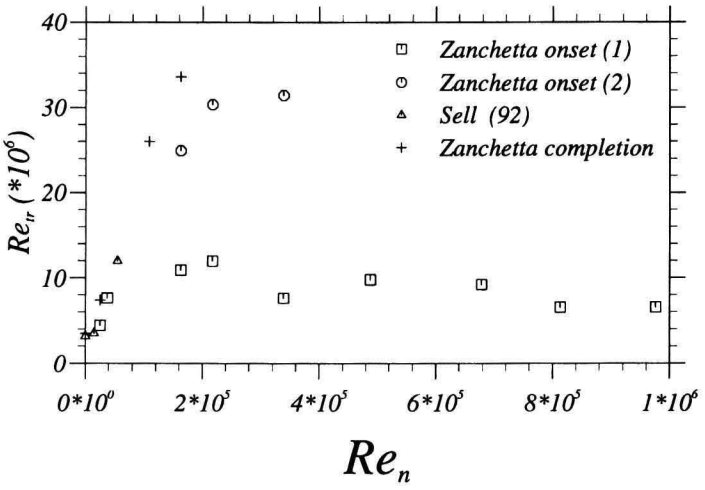

Figure 1: Transition Reynolds number versus nose Reynolds number.

Model

The basic model geometry is a five-degree semi-angle cone. A selection of interchangeable hemi-spherically blunted noses is used to obtain Re_n from 0 (nominally sharp) to 1 million. The model is equipped with 65 thin film gauges aligned along a generatrix of the cone. Prior to and during the run, the temperature evolution is sampled and stored digitally at 125 kHz and successively convoluted to obtain the time-resolved heat-transfer rate using the expression of Cook & Felderman (1966).

Transition in the pre-reversal regime

To illustrate the pre-reversal transition process, a test case with $Re_n = 2.4 \times 10^4$ has been selected. Time-resolved heat-transfer rates at five different streamwise locations in the laminar, transitional and turbulent regions are given in Fig. 2.

Gauge 02, located at the most upstream station, shows the typical laminar signal. The fluctuations arise mainly from digitisation and convolution noise. The boundary-layer edge properties at this location, as predicted by CFD, are given below:

s	δ	δ^*	θ	Re_{edge} (m^{-1})	M_e
0.361 m	2 mm	1.34 mm	0.07 mm	19.2 $\times 10^6$	7.69

At station 24, the appearance of transition events can be seen. Inspection of other time histories (which are not presented in Fig. 2) indicate that the first station at which the transition events are witnessed is gauge 06, (s = 0.385 m) giving Re_{tr}=4.73 $\times 10^6$. The high-frequency intermittent nature of the transition

process can be observed at gauge 34. Station 46 shows that the transition process is almost complete (other experiments show "stubborn regions" of laminar flow still persisting here). At the most downstream location (station 65) the boundary layer is believed to be fully developed turbulent. Again, inspection of time traces not included in Fig. 2, indicate that transition completion occurs at about gauge 60, $s = 0.69$ m, $Re_s = 8.47 \times 10^6$). In Fig. 3, the variation of time-averaged heat-transfer rate versus gauge location is given, together with the laminar CFD prediction. The mean heat-transfer rates can be seen to depart dramatically from the laminar trend given by the computation once the transition process begins, showing a local maximum (at $s = 0.6$ m) upstream of transition completion. Also of interest is the signal RMS, shown in Fig. 4. Although the inherent system noise has not been removed, the increase of signal RMS due to the onset of transition is obvious. The RMS reaches a certain peak value at a location corresponding to the steepest gradient in mean heat-transfer rate, thereafter decreasing to a turbulent RMS value greater than the laminar level. The intermittency distribution for this case, obtained using a threshold-type criterion, can be found in Fig. 5. The universal distribution based on the hypothesis of concentrated breakdown of Narasimha (1957) is also included in this plot. It is seen that it shows close agreement with the experimental data, except at the low levels of intermittency activity, where the experimental intermittency criterion is most prone to error. In Fig. 6, the PDF for selected gauges is given. The PDF for the "laminar" gauge (02) and the "turbulent" gauge (65) show a quasi Gaussian distribution, centred around the respective mean heating levels. The transitional gauges 24, 34 and 45 show the progressive re-arrangement of the PDFs with the advancement of the transition process.

Transition in the reversal regime

Visualisation experiments indicate that the reversal regime is characterised by sensitivity to roughness transition mechanisms. Experiments conducted with $Re_n = 1.08 \times 10^6$, illustrate the role of roughness in the hemispherical nose region. In Figs 7a and 7b, two liquid crystal visualisations are presented. In Fig. 7a, the nose region is polished to create a smooth surface and the boundary layer remains laminar over the entire model length ($Re_s > 3 \times 10^7$). In Fig. 7b, 50 μm mean diameter roughness elements are distributed uniformly over the nose region. Streak-like wake structures appear downstream of the sphere cone junction and undergo transition by $Re_s = 4 \times 10^6$. Heat-transfer measurements indicate that the turbulent events occurring in the reversal regime are characterised by a low-intermittency frequency (< 1 kHz).

The division between the pre-reversal and reversal regime is not distinct, and there exists a range of Re_n in which both mechanisms occur concurrently and "compete" to produce transition. In Fig. 8, the heat-transfer time trace for a "transitional gauge" can be seen. The nose Reynolds number is 1.26×10^5. Two types of transition events can be seen. The first are reversal regime events, marked X in Fig. 8, and originating in the nose and near nose region (x_{tb} in

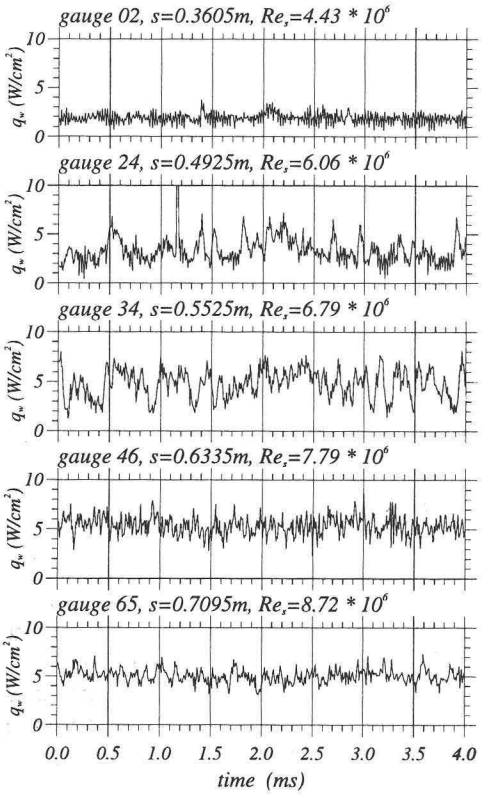

Figure 2: Time-resolved heat-transfer rates for five selected gauges, $Re_n = 2.4 \times 10^4$.

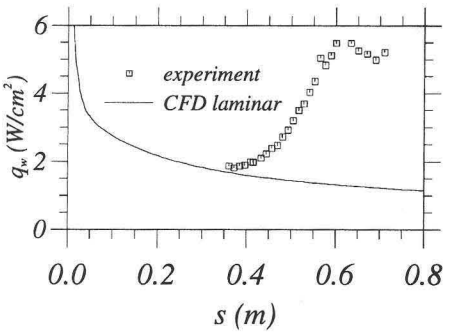

Figure 3: Time-average heat-transfer rate versus wetted distance, $Re_n = 2.4 \times 10^4$.

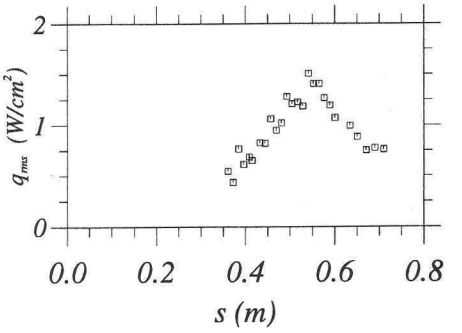

Figure 4: RMS heat-transfer rate versus wetted distance, $Re_n = 2.4 \times 10^4$.

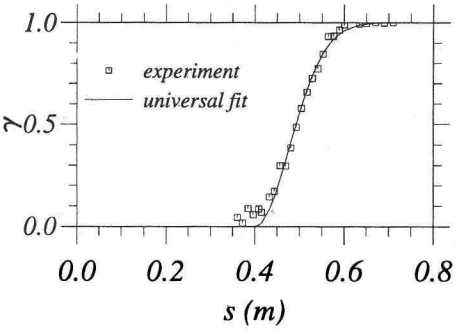

Figure 5: Intermittency versus wetted distance, $Re_n = 2.4 \times 10^4$.

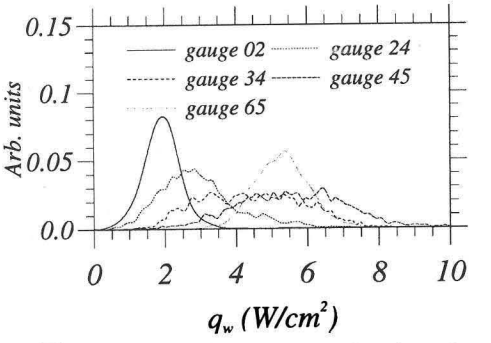

Figure 6: Probability density function, $Re_n = 2.4 \times 10^4$.

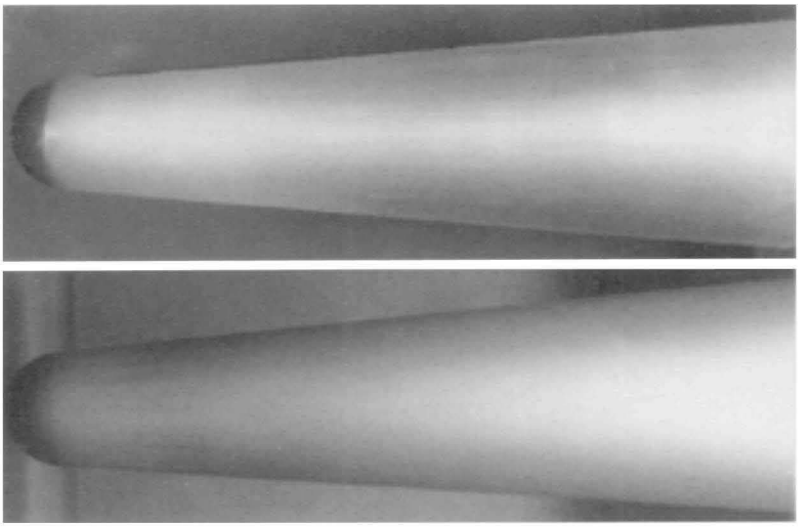

Figure 7: Liquid crystal visualisation, $Re_n = 1.08 \times 10^6$; (a) smooth nose, (b) rough nose.

Fig. 9). The second are transition spikes caused by the pre-reversal transition mechanism starting at x_{ts}. In this particular case, after the onset of the pre-reversal mode, (s = 0.4 m Re_s =16.8 $\times 10^6$; found by inspection of the time histories not presented here), transition occurs rapidly. The occurrence of this transition mode is also highlighted by an abrupt rise in the transition event passage frequency, Fig. 10, reaching a maximum in excess of 5 kHz at s = 0.52 m which is found to be the 50% intermittency location.

Reversal regime transition events

The reversal regime transition event with its characteristic low frequency (< 1 kHz) and large spatial scales (> 100 mm) is reasonably well resolved by the sensors and A/D equipment. For the Re_n=1.26$\times 10^5$ test case, the leading and trailing edge passage times for events have been tracked, using the time-history data, at 5 stations upstream of s = 0.4 m ($Re_s = 1.68 \times 10^7$). These are depicted in Fig. 11, and indicate for the leading and trailing edges speeds of 94% and 63% of the boundary layer edge velocity respectively. This information is included in the illustration of Fig. 12. Estimates for the mean-event convection speeds, evaluated using the cross-spectral density function and the correlation functions, are of 71% and 82% of the edge velocity respectively.

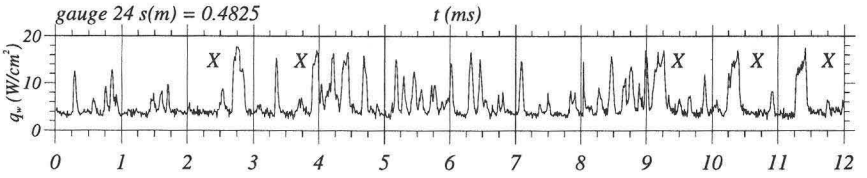

Figure 8: Time-resolved heat-transfer rates, gauge 24, $Re_n = 126,000$. X indicates reversal regime transition events.

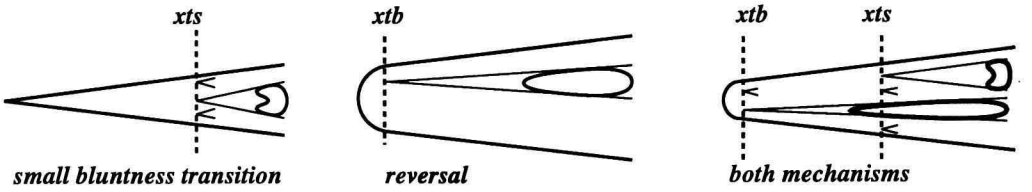

Figure 9: Schematics of transition dynamics.

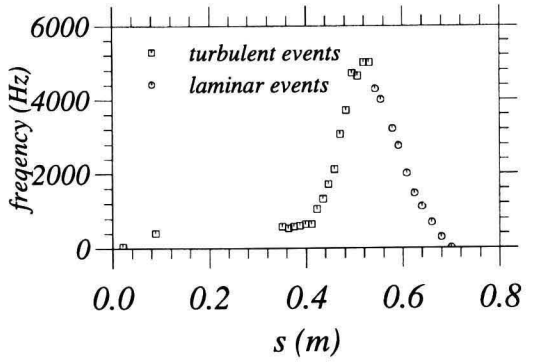

Figure 10: Turbulent event passage frequency versus wetted distance for $Re_n = 1.26 \times 10^5$.

Conclusion

In this paper, pre- and transition reversal regimes have been explored. The experiments indicate that transition in the pre-reversal is characterised by the breakdown of the laminar boundary layer at some streamwise location. Transition completion occurs by a high-frequency formation and subsequent growth of turbulent events. Increasing Re_n moves the point of breakdown further downstream. In the reversal regime, low-frequency turbulent events are formed in the nose and near nose region. The formation rate (spatial and temporal) is dependent on the severity of the roughness environment in the hemispherical nose region. The "reversal" event has a streamwise length in excess of 100δ and leading and trailing edge speeds of 94% and 63% of the edge velocity respectively.

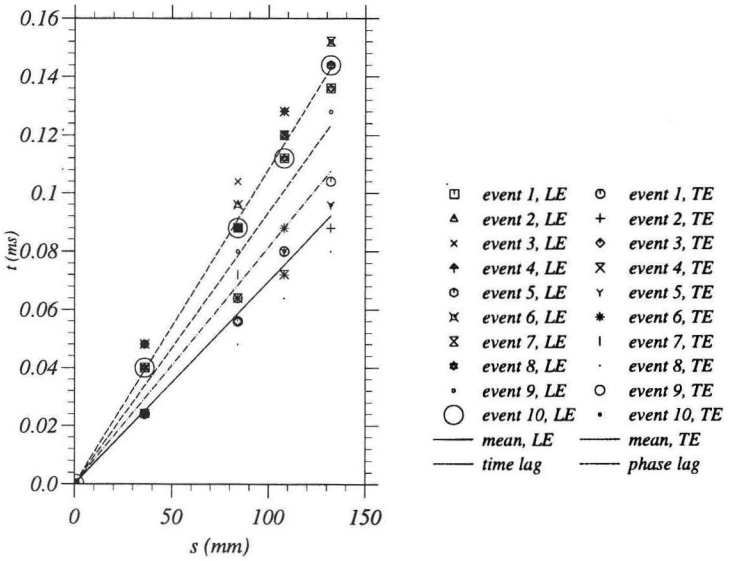

Figure 11: Transition event trajectories. Data obtained at five stations for the Re_n = 1.26 x 10^5 test case.

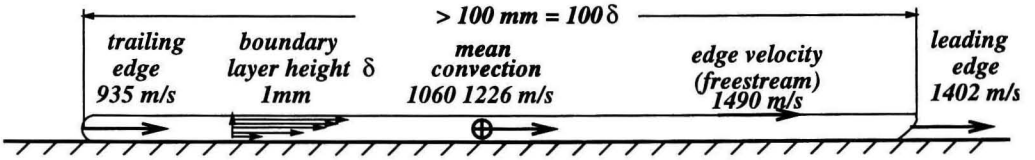

Figure 12: Quasi one dimensional illustration of a turbulent event.

Acknowledgements

This work was funded by the Defence Research Agency. The authors wish to thank Mr. S. Johnson and Mr. R. Hutchins of Imperial College and acknowledge the support and guidance of Dr. T. Caine, Dr. M. Collyer, Dr. M. Gilmore and Dr. I. Wrisdale of DRA Farnborough.

References

Cook, W.J. & Felderman, E.J. 1966 – Reduction of data from thin film heat transfer gauges. A concise numerical technique. *AIAA* **4**, 561-562.

Narasimha, R. 1957 – On the distribution of intermittency in the transition region of a boundary layer. *J. Aer. Sci.* bf 24, 711-712.

Sell, M. 1992 – Hypersonic blunt cone aerodynamics. *Ph.D. thesis University of London.*

Authors' address

Department of Aeronautics, Imperial College of Science,
Technology and Medicine. SW7 2BY, London, U.K.